

## Escape of H and D from Mars and Venus by energization with hot oxygen

Bernic D. Shizgal<sup>1</sup>

Communications Research Laboratory, Tokyo

**Abstract.** A kinetic theory collisional production model is used to determine the product velocity distributions of H and D resulting from collisional energy transfer with hot oxygen. The energetic oxygen atoms are the products of the dissociative recombination of  $O_2^+$ . Quantum mechanical cross sections for O-H and O-D collisions are used to determine the production distributions. The distributions of the particles entering a collision are assumed to be Maxwellian functions. The fraction of atoms with speeds above the escape speed is determined for Venus and Mars. For Venus, available density and temperature profiles are used to obtain estimates of the H and D escape fluxes and fractionation ratios.

### 1. Introduction

There are numerous processes in the terrestrial atmosphere and atmospheres of other planets, notably Mars and Venus, which involve the production of translational energetic atoms with energies considerably above thermal energies. These “hot” atoms can play an important role in enhanced reaction rates [Logan and McElroy, 1977; L e-Svendsen et al., 1991; Shizgal and Lindenfeld, 1979], nonthermal emissions [Whipple et al., 1975; Armstrong et al., 1994], and, in particular, the enhanced nonthermal escape of atmospheric species [Shizgal and Arkos, 1996; Hunten, 1991; Fahr and Shizgal, 1983]. Photodissociation of  $O_2$  and  $O_3$  produces a population of energetic  $O(^1D)$  [Logan and McElroy, 1977; Shizgal and Lindenfeld, 1979], which can react with other atmospheric species producing an abundance of other free radicals. Energetic  $O(^1S)$  atoms are produced by dissociative recombination of  $O_2^+$ . Metastable  $O(^1S)$  are the source of the 5577 Å green line emission in the F region of the thermosphere [Hays and Walker, 1971; Whipple et al., 1975; Yee and Dalgarno, 1985]. Similarly, ion-molecule reactions can produce energetic nitrogen atoms, and these can play an important role in atmospheric nitrogen chemistry [L e-Svendsen et al., 1991; Kharchenko et al., 1997; G erard et al., 1997]. Exothermic chemical reactions in the Martian atmosphere can produce nonthermal distributions of oxygen and nitrogen atoms and lead to enhanced escape of these species [Fox, 1993; Fox and Hac, 1997a,b].

On the terrestrial planets, there are several processes that lead to the production of substantial populations of energetic atoms that can have energies above the escape speed of the planet. These nonthermal escape mechanisms play an important role in the evolution of the atmospheres of these planets [Shizgal and Arkos, 1996]. The charge exchange process of energetic  $H^+$  or  $D^+$  in collision with neutral H can produce a significant population of H and D atoms with energies well above thermal [Chamberlain, 1977; Shizgal and Lindenfeld, 1982; Hodges and Breig, 1991, 1993; Hartle et al., 1996]. The dissociative recombination of  $O_2^+$  can produce energetic oxygen atoms on all three terrestrial planets, and substantial coronae of hot oxygen are expected on Earth, Mars, and Venus [Ip, 1988; Lammer and Bauer, 1991]. These energetic oxygen atoms can transfer their energy to H and D and create additional energetic populations of H and D [Cooper et al., 1984; Gurwell and Yung, 1993].

The existence of extended corona of energetic H and O in the atmospheres of the terrestrial planets is now well established, both from theoretical models and observations. There is a continued interest in a better understanding of the physics of the processes that produce and maintain these steady state, nonequilibrium distributions. In the rarefied atmosphere of the high-altitude portions of these planetary atmospheres, collisional relaxation of nonthermal distributions is slow. The extent of the departure from equilibrium distributions depends on the strengths of the processes that perturb the distributions from equilibrium and the collisional relaxation processes that restore the distributions to Maxwellians. If there is a significant population of energetic atoms with speeds in excess of the escape speed of the planet, these extended corona can have an important effect on the rate of loss of atmospheric species, both directly and indirectly. The indirect loss usually involves the inter-

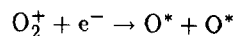
<sup>1</sup>Now at Departments of Chemistry and Physics, University of British Columbia, Vancouver, Canada. (shizgal@theory.chem.ubc.ca)

Copyright 1999 by the American Geophysical Union.

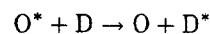
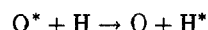
Paper number 1999JA900157.  
1048-0227/99/1999JA900157\$09.00

action of the corona of neutral atoms with the plasma of the solar wind. A detailed review of these nonthermal processes has been presented in a recent review [Shizgal and Arkos, 1996].

In this paper, we consider the dissociative recombination of  $O_2^+$  producing energetic oxygen atoms,  $O^*$ , that is,



where there are several different channels possible with the product oxygen atoms in different electronic states [Guberman, 1988; Fox and Hac, 1997b]. This is an important nonthermal process that has been considered in the modeling of the hot oxygen coronae in the atmospheres of the terrestrial planets [Knudsen, 1973; Ip, 1988; Lammer and Bauer, 1991; Nagy et al., 1981, 1990]. There is also an analogous process involving  $N_2^+$  [Wallis, 1978; Lammer and Bauer, 1991; Fox and Hac, 1997a, b]. The main objective of this paper is to reexamine the role of these energetic O atoms in energizing H and D and the creation of nonthermal populations via the elastic energy exchange processes,



The important aspect of these nonthermal processes is the extent of the nonthermal distributions of the product H and D and the subsequent escape fluxes from Mars and Venus.

This mechanism has a very long history in the discussion of atmospheric escape [Knudsen, 1973; Wallis, 1978]. McElroy and coworkers [McElroy et al., 1982; Rodriguez et al., 1984] suggested that this process would be 100% selective for H escape against D escape. Cooper et al. [1984] studied the dynamics of O-H collisions with standard quantum mechanical methods and estimated the fraction of the product H atoms that would have energies above the escape energy. They did not consider O-D collisions, nor did they provide estimates of escape fluxes. In their calculations of escape fractions, they also assumed that the distribution of oxygen atoms produced from dissociative recombination is a delta function at 2.5 eV, the exothermicity of the dissociative recombination reaction. The distribution function of the product atoms is certainly not a delta function and is broadened by collisions. Gurwell and Yung [1993] determined the distribution function of the product oxygen atoms from a simulation and used this as input to estimate the extent of the energization of H and D by hot oxygen. The cross sections for both O-H and O-D collisions were taken to be the same, which is not correct. The important dynamical isotope effect in the cross sections [Shizgal, 1999] was not taken into account. They also based their calculation on the differential cross section at a single collision energy taken from the paper by Cooper et al. [1984]. Thus the energy dependence of the process was not properly considered.

Hodges [1993a] repeated the quantum calculations of O-H and O-D collisions performed earlier by Cooper et al. [1984] and found several discrepancies in the final results for the cross sections. A thorough study of the interaction potentials for O-H and an analysis of the quantum calculations of O-H and O-D collisions was recently reported by Shizgal [1999] with results that differ from the previous work of Cooper et al. [1984] and Hodges [1993a]. The differences were attributed to the interpolation procedure used to match the tabulated potentials and the analytic, long-range behavior. Hodges [1993a] did not consider the calculation of H and D energization or estimates of escape fluxes. Hodges [1993b] has subsequently suggested that the escape of H from impact energization by hot O is not an important process. He based this conclusion on the comparison of O distributions resulting from dissociative recombination with and without O-O\* collisions. He refers to O\* distribution functions that result directly from dissociative recombination as "primitive" distributions. With the inclusion of O-O\* collisions, he found a strong diminution of the hot energy "tail" of the O\* distribution functions from the primitive distributions, which is not surprising. Hodges [1993b] concluded from this observation that escape of H by O impact is unimportant, also discussed by Hartle et al. [1996] and Donahue et al. [1997]. However, Hodges [1993b] did not calculate H and D escape fluxes with both sets of hot oxygen distributions, and the observation that the partial thermalization of the oxygen hot energy tail mitigates against escape by this mechanism is inconclusive. A more detailed calculation of the escape fluxes is required to definitively eliminate O impact as an important process.

In this paper, the updated quantum mechanical cross sections for both O-H and O-D collisions reported by Shizgal [1999] are used to calculate the nonthermal distributions of product H and D. The product velocity distribution functions of H and D are calculated as described in section 3. As discussed there, the calculation of escape fluxes involves detailed, self-consistent distribution functions in velocity or speed and altitude. In this paper, the distribution functions of O\* and H (or D) entering a collision are assumed to be Maxwellian. For O\*, the temperature varies with altitude, and this variation indirectly reflects the thermalization of hot O\*. Estimates of escape fractions are given for specific temperature ratios of H and O\*.

It is demonstrated that the detailed angular anisotropy of the differential elastic cross sections is very important in the energization process and the calculation of escape fluxes. This was first pointed out by Shizgal [1985, 1987] in connection with charge exchange collisions and later confirmed by Hodges and Breig [1993]. Gurwell and Yung [1993] have also shown that for O-H collisions the dependence of the differential cross sections on the scattering angle is very important. Kharchenko et al. [1997] also recently demonstrated the importance of taking into account the detailed anisotropy of the

differential cross sections in O-N collisions. These are not surprising results since the comparison of calculated and measured transport coefficients have always required accurate, differential cross sections [Viehland, 1994]. Isotropic, hard sphere cross sections provide useful estimates, but it is often difficult to know the value of the hard sphere cross section that fits the results obtained with the actual differential cross sections [Karchenko *et al.*, 1997].

The determination of the escape flux requires an integration of the local escape rates at a given altitude over a range of altitudes in the vicinity of the exobase. The density profiles for O\* and H (as well as for D) are required. In section 2 of the paper, the Boltzmann equation for the distribution of hot atoms is presented to motivate the derivation of the product velocity distribution functions in section 3. The formalism of section 3 is applied to the energization of H and D by energetic oxygen on Venus and Mars in section 4. A discussion of the calculation of the escape fluxes of H and D from Venus is discussed in section 5. With the assumption that the distribution of hot oxygen entering a collision is a Maxwellian, the most important quantity in these calculations is the temperature of the hot oxygen. This will vary with altitude being equal to the thermal background temperature and increasing dramatically at altitudes near the exobase, where collisional thermalization is no longer effective. The temperature of hot oxygen is assumed to be given by the local scale height of hot oxygen density distributions previously reported in the literature. In the appendix, an approximate solution of the Boltzmann equation is presented to provide a qualitative description of the thermalization effects. These profiles are compared with the profile extracted from the distributions obtained with Monte Carlo simulations by Hodges [1993b].

## 2. Boltzmann Equation and Collision Frequencies

The rigorous kinetic theory treatment of the coupled dissociative recombination and energy transfer processes discussed in section 1 involves the solution of several coupled Boltzmann equations for the distributions of all species. This would take into account the production of energetic oxygen atoms and the subsequent thermalization by collisions with ambient species. The approach adopted here is to assume that the product oxygen atoms are Maxwellian with some altitude dependent temperature. The main objective is to determine the distributions of the product H\* (and D\*) after collision with O\*.

In this section, the detailed calculations of section 3 are put into context in terms of an analysis based on the Boltzmann equation. This Boltzmann equation is also considered for the calculations in the appendix. The local Boltzmann equation of some energetic species labeled 1 in collision with a second species labeled 2

(which is taken in large excess relative to species 1) is of the form [Chapman and Cowling, 1970; Gombosi, 1994]

$$\frac{\partial f_1(\mathbf{r}, \mathbf{v}_1, t)}{\partial t} = J[f_1(v_1, t)] + S(v_1) \quad (1)$$

where  $S(v_1)$  is some source of hot atoms of type 1. The effect of collisions between species is taken into account in the collision operator,  $J[f_1(v_1, t)]$ , defined by,

$$J[f_1] = \iint [f_1(v'_1, t)f_2^{(M)}(v'_2) - f_1(v_1, t)f_2^{(M)}(v_2)] \times g\sigma(g, \theta)d\Omega dv_2 \quad (2)$$

where the Maxwellian distribution for species 2 is given by  $f_2^{(M)}(v_2) = N_2(\sqrt{\lambda_2}/\pi)^3 \exp(-\lambda_2 v_2^2)$  with  $\lambda_2 = m_2/2k_B T_2$ . In (2),  $\sigma(g, \theta)$  is the differential cross section for collisions between species 1 and 2, which depends on the relative speed,  $g$  ( $\mathbf{g} = \mathbf{v}_2 - \mathbf{v}_1$ ) and the center-of-mass scattering angle  $\theta$ . The purpose of this discussion is to introduce the collision operator, (2). It is composed of two terms: a gain term with the primed velocities (the postcollisional velocities) and a loss term without the primed velocities (the precollisional velocities). The role of the source function,  $S(v_1)$ , is discussed in the appendix.

The second term in the collision operator of (2) can be written in terms of the velocity dependent collision frequency, which is denoted by

$$Z_{(-)}(v_1) = \iint f_2^{(M)}(v_2)g\sigma(g, \theta)d\Omega dv_2 \quad (3)$$

which can also be written in terms of the total elastic cross section; that is,

$$Z_{(-)}(v_1) = \int f_2^{(M)}(v_2)g\sigma_{\text{tot}}(g)dv_2 \quad (4)$$

If the cross section is a hard sphere cross section,  $\pi d^2$ , independent of energy, the collision frequency can be determined analytically and the result is well known [Chapman and Cowling, 1970; Shizgal and Fitzpatrick, 1975] and given by

$$Z_{(-)}^{(\text{hs})}(v_1) = N_2 d^2 \sqrt{2\pi k_B T_2 / m_2} [e^{-\lambda_2 v_1^2} + \frac{\sqrt{\pi}}{2} (\frac{1}{\sqrt{\lambda_2 v_1}} + 2\sqrt{\lambda_2} v_1) \text{erf}(\sqrt{\lambda_2} v_1)] \quad (5)$$

where  $\text{erf}(x)$  is the error function. The total collision frequency is therefore given by

$$Q^{(\text{hs})} = \int f_1(\mathbf{v}_1) Z_{(-)}^{(\text{hs})}(v_1) d\mathbf{v}_1 \quad (6)$$

If  $f_1(\mathbf{v}_1)$  is taken as a Maxwellian with a temperature  $T_1 \neq T_2$ , then

$$Q^{(\text{hs})} = N_1 N_2 \pi d^2 \sqrt{\frac{8k_B T_{\text{eff}}}{\pi \mu}} \quad (7)$$

where the effective temperature is a mass-weighted temperature,  $T_{\text{eff}} = (m_1 T_1 + m_2 T_2) / m_0$  with  $m_0 = m_1 +$

$m_2$  and the reduced mass  $\mu = m_1 m_2 / m_0$ . The number densities of species 1 and 2 are denoted by  $N_1$  and  $N_2$ , respectively.

The gain term is more involved since it is determined by the angular dependence of the differential cross section in addition to the relative speed (or energy) dependence. This gain term or production function is

$$f_1^{(M)}(v_1) Z_{(+)}(v_1) = \iint f_1(\mathbf{v}_1') f_2^{(M)}(v_2') g \sigma(g, \theta) d\Omega d\mathbf{v}_2 \quad (8)$$

It is clear that the two collision frequencies  $Z_{(+)}(v_1)$  and  $Z_{(-)}(v_1)$  are very different. However, from particle conservation we have that

$$Q = \int f_1(v_1) Z_{(-)}(v_1) d\mathbf{v}_1 = \int f_1(v_1) Z_{(+)}(v_1) d\mathbf{v}_1 \quad (9)$$

Equation (8) gives the rate of production of product atoms. The speed distribution of these product atoms, without subsequent thermalization, is then given by

$$P(v) = \frac{f_1^{(M)}(v_1) Z_{(+)}(v_1)}{Q} \quad (10)$$

In analogy with (5), the result for the gain collision term for the hard sphere cross section and both distribution functions assumed to be Maxwellian at two different temperatures was derived by *Shizgal and Fitzpatrick* [1975] and given by

$$Z_{(+)}^{(hs)}(v_1) = \frac{N_2 \pi d^2}{4M_1 M_2 \tau (\lambda_1 v_1)} [h_2 \exp(h_1 \lambda_1 v_1^2) + \text{erf}(h_2 \sqrt{\lambda_2} v_1) - \text{erf}(\sqrt{\lambda_2} v_1)] \quad (11)$$

where  $h_1 = 4M_1 M_2 \tau / (1 + 4M_1 M_2 \tau)$ ,  $h_2 = (1 + 2M_1 \tau) / \sqrt{1 + 4M_1 M_2 \tau}$ ,  $\tau = (T_2/T_1 - 1)$ ,  $M_1 = m_1 / (m_1 + m_2)$ , and  $M_2 = m_2 / (m_1 + m_2)$ . Equation (11) gives the rate of production of the products of an elastic collision with the particles entering the collision given by Maxwellians at different temperatures, and the cross section is a hard sphere cross section. If  $T_1 \rightarrow T_2$ , then  $Z_{(+)}(v_1) \rightarrow Z_{(-)}(v_1)$ . Equation (11) was the basis for the simple model for charge exchange-induced escape of terrestrial hydrogen by *Shizgal and Lindenfeld* [1982]. *Whipple* [1974] has presented a very detailed discussion of the use of different distribution functions in (8) in the determination of  $Z_{(+)}(v_1)$  for reactive collisions for which energy is not conserved. Equation (10) could be used to determine the product velocity distribution of energetic oxygen as a result of dissociative recombination or for the distribution of  $H^*$  (or  $D^*$ ) following an energy exchange elastic collision, which is the objective here.

### 3. Two Temperature Product Velocity Distribution Functions

The main objective of this paper is the determination of the product velocity distributions immediately after

elastic collisions ( $O^*$ , H) and ( $O^*$ , D), where both species entering the collision are described by Maxwellian distributions at different temperatures. In addition to the activation of H and D by energetic oxygen impact, it also has other potential applications to the study of the product velocity distributions in ( $H^+$ , H) and ( $D^+$ , H) charge exchange collisions studied in a subsequent publication. *Cooper et al* [1984] calculated the product velocity distributions for H with energetic O impacting on H with a delta function for the O distribution and a Maxwellian for the initial H distribution. The choice of Maxwellian distributions for both species is similar to the approach adopted by *Gurwell and Yung* [1993], *Hodges and Breig* [1993], and *Fox and Hać* [1997a, b].

The product velocity distributions are determined from the loss term of the Boltzmann equation, (8), which can be written as

$$f_1^{(M)}(v_1) Z_{(+)}(v_1) = N_1 N_2 \left( \frac{\sqrt{\lambda_1 \lambda_2}}{\pi} \right)^3 \times \iint e^{-\lambda_1 v_1'^2 - \lambda_2 v_2'^2} g \sigma(g, \Omega) d\Omega d\mathbf{v}_2 \quad (12)$$

We change variables from  $\mathbf{v}_2$  to  $\mathbf{g}$  ( $\mathbf{v}_2 = \mathbf{g} + \mathbf{v}_1$ ) with  $\mathbf{v}_1$  fixed and write

$$f_1^{(M)}(v_1) Z_{(+)}(v_1) = N_1 N_2 \left( \frac{\sqrt{\lambda_1 \lambda_2}}{\pi} \right)^3 \times \iint e^{-\lambda_1 v_1'^2 - \lambda_2 v_2'^2} g^3 \sigma(g, \Omega) d\Omega d\Omega' dg \quad (13)$$

The solid angles  $\Omega$  and  $\Omega'$  give the orientations of  $\mathbf{g}'$  and  $\mathbf{v}_1$  about the direction of  $\mathbf{g}$ , taken as the polar axis.

The individual particle velocities can be expressed in terms of the center-of-mass velocity,  $\mathbf{G} = M_1 \mathbf{v}_1 + M_2 \mathbf{v}_2$ , and relative velocity,  $\mathbf{g} = \mathbf{v}_2 - \mathbf{v}_1$ . The primed velocities that occur in (13) can be obtained from these equations and with conservation of momentum,  $\mathbf{G}' = \mathbf{G}$ . If  $\mathbf{G}$  is eliminated from these equations, we have that  $\mathbf{v}_1' = \mathbf{v}_1 + M_2(\mathbf{g} - \mathbf{g}')$  and  $\mathbf{v}_2' = \mathbf{v}_1 + M_1 \mathbf{g}' + M_2 \mathbf{g}$ . Hence, with conservation of energy  $g = g'$ , the argument of the exponential term in (13) can be written in the form

$$\lambda_1 v_1'^2 + \lambda_2 v_2'^2 - A v_1^2 + D g^2 + \alpha \mathbf{v}_1 \cdot \mathbf{g} + \beta \mathbf{v}_1 \cdot \mathbf{g}' + \gamma \mathbf{g} \cdot \mathbf{g}' \quad (14)$$

where  $A = \lambda_1 + \lambda_2$ ,  $B = 2M_2^2 \lambda_1 + (M_1^2 + M_2^2) \lambda_2$ ,  $\alpha = 2M_2(\lambda_1 + \lambda_2)$ ,  $\beta = 2(M_1 \lambda_2 - M_2 \lambda_1)$ , and  $\gamma = 2M_2(M_1 \lambda_2 - M_2 \lambda_1)$ . If one examines the form of (14) and the integrations in (13), it is clear that  $Z_{(+)}(v_1)$  can be reduced to a two-dimensional integral over the relative speed  $g$  and the scattering angle  $\theta$  and involves the differential scattering cross section. These two integrations must be done numerically, except for model cross sections. Hence, with (14) in (13), we have that

$$f_1^{(M)}(v_1) Z_{(+)}(v_1) = N_1 N_2 \left( \frac{\sqrt{\lambda_1 \lambda_2}}{\pi} \right)^3 e^{-A v_1^2} \times \int_0^\infty \int_{-1}^1 e^{-B g^2 - \gamma g^2 \cos \theta} K(g, \theta) \sigma(g, \Omega) g^3 d(\cos \theta) dg \quad (15)$$

The remaining integrations, which can be done analytically, are collected in  $K(g, \theta)$ , defined by

$$K(g, \theta) = \int_{\Omega'} \int_0^{2\pi} \exp[-\alpha \mathbf{v}_1 \cdot \mathbf{g} - \beta \mathbf{v}_1 \cdot \mathbf{g}'] d\phi d\Omega'$$

$$K(g, \theta) = 2\pi \int_{-1}^1 \int_0^{2\pi} \exp[-\alpha v_1 g \cos \theta' - \beta v_1 g \times (\cos \theta \cos \theta' + \sin \theta \sin \theta' \cos \phi)] d\phi d(\cos \theta')$$
(16)

where the addition theorem has been used to express the cosine of the angle between  $\mathbf{v}_1$  and  $\mathbf{g}$  in terms of  $\theta$ ,  $\theta'$  and  $\phi$ . The  $\phi$  integral can be expressed in terms of a Bessel function,  $I_0(z) = (1/\pi) \int_0^\pi \exp(-z \cos \phi) d\phi$ . With this result and the definitions of the coefficients  $D_1 = \alpha g c_1 + \beta g c_1 \cos \theta$  and  $D_2 = \beta g c_1 \sin \theta$  of  $\cos \theta'$  and  $\sin \theta'$ , respectively, we have that

$$K(g, \theta) = (2\pi)^2 \int_{-1}^1 e^{-D_1 \cos \theta'} I_0(D_2 \sin \theta') d(\cos \theta')$$

$$K(g, \theta) = 2(2\pi)^2 \frac{\sinh \sqrt{D_1^2 + D_2^2}}{\sqrt{D_1^2 + D_2^2}} \quad (17)$$

With  $D_1^2 + D_2^2 = g^2 v_1^2 (\alpha^2 + \beta^2 + 2\alpha\beta \cos \theta)$  we get the final desired result.

$$f_1^{(M)}(v_1) Z_{(+)}(v_1) = N_1 N_2 \left( \frac{\sqrt{\lambda_1 \lambda_2}}{\pi} \right)^3 2(2\pi)^2 \frac{e^{-A v_1^2}}{v_1}$$

$$\times \int_0^\infty \int_0^\pi e^{-B g^2 - \gamma g^2 \cos \theta} \sigma(g, \theta) g^2 \sin^2 \theta$$

$$\times \frac{\sinh(g v_1 \sqrt{\alpha^2 + \beta^2 + 2\alpha\beta \cos \theta})}{\sqrt{\alpha^2 + \beta^2 + 2\alpha\beta \cos \theta}} d\theta dg \quad (18)$$

This result is used in the section immediately following in the calculation of the  $\text{H}^*$  and  $\text{D}^*$  energetic distributions resulting from dissociative recombination and subsequent energization with hot oxygen. *Hodges* [1993b] and *Hodges and Breig* [1991] evaluate similar collisional integrals with a Monte Carlo procedure, which is unnecessary. Equation (18) requires a two-dimensional integration, which can be done efficiently and accurately.

#### 4. Energization of H and D by Hot Oxygen: Escape Fractions for Venus and Mars

The product velocity distribution functions of H and D by collisions with energetic O based on Maxwellian distributions for the incident atoms, given by (10) and (18), were employed in the present work. These calculations are based on the detailed quantum mechanical cross sections for O-H and O-D collisions [Shizgal, 1999]. Figure 1 shows the differential cross sections for O-H collisions at two energies, 0.5 eV and 1.0 eV. The very sharp, forward scattering peak is clearly evident. The energy variation of the total cross section is shown

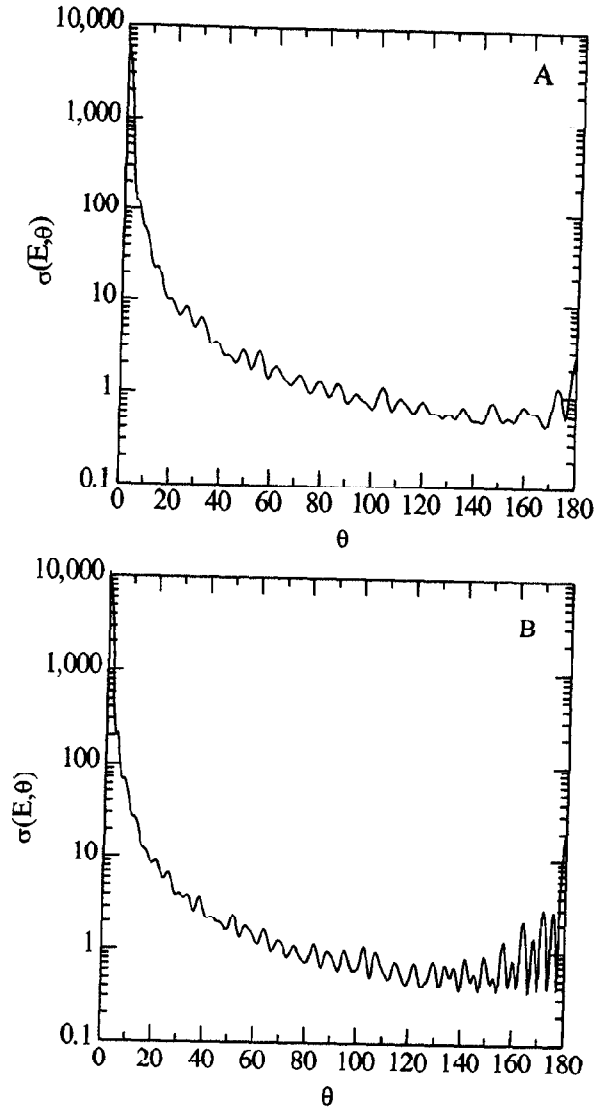
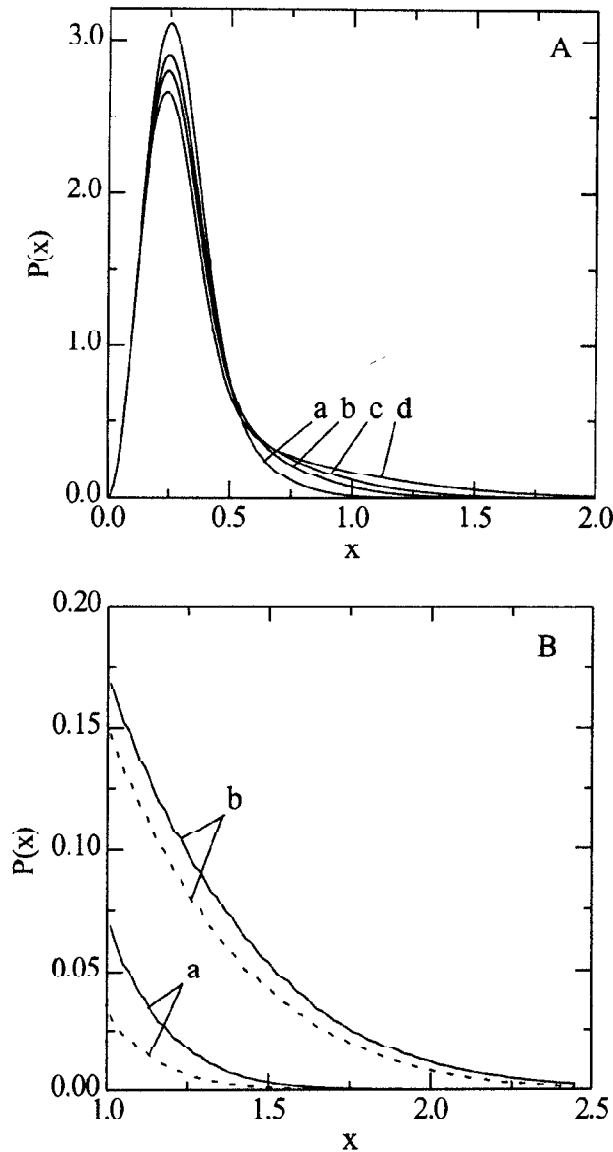


Figure 1. Differential cross sections (in  $\text{\AA}^2$ ) for O-H collisions at energy (a)  $E = 0.5$  eV and (b)  $E = 1.0$  eV.

in Figure 9 of *Shizgal* [1999], and there is a distinct isotope effect for O-H and O-D collisions. This effect was ignored in the work by *Gurwell and Yung* [1993]. Since the product velocity distribution functions are determined from the average of both angle and energy of the differential cross sections (equation (18)), both dependencies play an important role.

The product velocity distribution functions for H atoms on Venus, defined by (10) and (18), are shown in Figure 2 versus speed relative to the escape speed ( $x = v/v_{esc}$ ). Particles with reduced energies greater than unity are those that can escape. The distributions in Figure 2a are for  $T_H = 300$  K characteristic of the dayside exospheric temperature and increasing oxygen temperature as noted in the caption. The generation of a high-energy "tail" is clear, which is shown on an expanded scale in Figure 2b. Here the solid curves



**Figure 2.** The product velocity distribution function of H atoms for Venus that results from O-H collisions;  $x = v/v_{esc}$ . Temperatures  $T_H = 300$  K and (a)  $T_O$  is equal to 5,000 K (curve a), 10,000 K (curve b), 15,000 K (curve c), and 29,113 K (curve d). Product velocity distribution functions for energies above the escape energy. Solid curves are for O-H collisions, and dashed curves are for O-D collisions;  $T_O$  is equal to 10,000 K (curve a) and 29,113 K (curve b).

are for O-H collisions, whereas the dashed curves are for O-D collisions. Significant populations above the escape energy can be created, provided the oxygen temperature is sufficiently high; that is, there is a significant non-thermal oxygen distribution. The distributions shown in Figure 2 are normalized to unity.

Satellite measurements of the exosphere of Venus have clearly shown hydrogen atom distribution func-

tions characterized by two scale heights presumably from two populations of H atoms, one cold and the other hot. In Figure 3, the distribution functions are replotted versus energy in eV and taking out the  $x^2$  weight of the three-dimensional velocity volume in  $dx$ . The same  $T_H$  and  $T_O$  values as in Figure 2 were used, and the slopes of the linear portions of the curves in Figure 3 at low and high energies give the temperatures noted in the caption. This is a demonstration of the two temperature exosphere.

In Figure 4, similar results for Mars are shown (curves a and b), except that the fraction of particles above the escape energy is larger. The distributions for both planets with the present model are the same. The difference arises from the definition of the reduced energy taken relative to the escape energy, which is smaller for Mars. Curves c and d in Figure 4 are the results with the total isotropic cross section replaced with the total isotropic cross section, i.e.,  $\sigma(E, \theta)$  given by  $\sigma_{tot}(E)/4\pi$ . As can be seen from a comparison of curves a and b with curves c and d, the detailed angular distribution is very important in the energization of the products. The isotropic cross section overestimates the high-energy portion of the distribution. The dashed curves are the distributions obtained with hard sphere cross diameters of 4.92 Å (curve e) and 4.63 Å (curve d), obtained by fitting the collision rates given by (19) to (7).

The total collision rate with the incident particles described by Maxwellians at temperatures  $T_1$  and  $T_2$  is given by

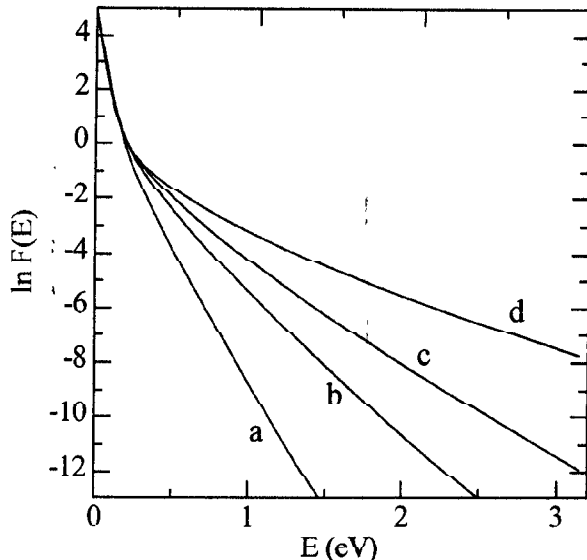


**Figure 3.** Variation of  $\ln F(E) = \ln[P(x)/x^2]$  versus energy  $E$  in eV. The distribution function shows an approximately bi-Maxwellian behavior, characterized by two temperatures given by the slopes of the linear portions of the curve.  $T_O$  values are same as in Figure 2. The cold temperature is about 420 K, whereas  $T_{hot}$  is equal to 1300 K (curve a), 2300 K (curve b), 3200 K (curve c), and 5400 K (curve d).

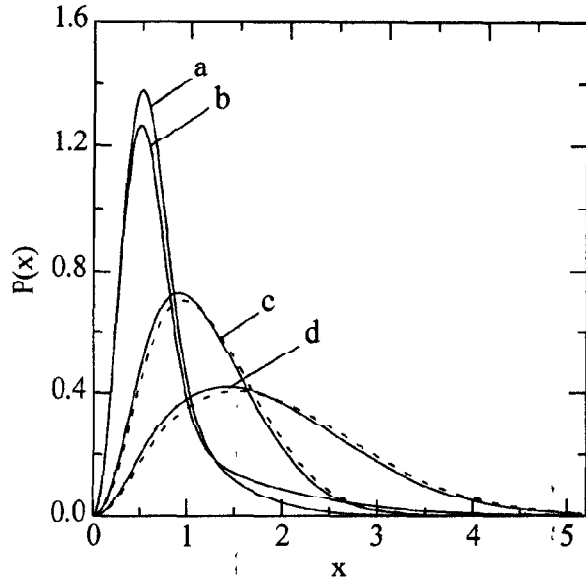


Figure 4. Product velocity distributions of H on Mars.  $T_H = 300$  K and  $T_O = 10,000$  K (curve a) and  $29,113$  K (curve b), both calculated with the differential cross section. Curves c and d are the corresponding results with  $\sigma(E, \theta) = \sigma_{tot}(E)/4\pi$ . The dashed curves are the results with the hard sphere diameters  $4.92$  Å (curve c) and  $4.63$  Å (curve d), determined by fitting to the collision rate  $\hat{Q}$  in Table 1; see equation (7).

$$Q(T_{eff}) = N_O N_H \sqrt{\frac{8kT_{eff}}{\pi\mu}} \int_0^\infty e^{-y} \sigma_{tot}(y k_B T_{eff}) y dy \quad (19)$$

where  $y = E/kT_{eff}$  and  $\sigma_{tot}(E)$  is the total cross section. This reduces to (7) for a hard sphere cross section. The rate for escape is given by an integral similar to (9) [with  $Z_{(+)}(v_1)$ ] but with limits from the escape speed to infinity; that is,

$$R_{esc} = 4\pi \int_{v_{esc}}^\infty f(v) Z_{(+)}(v) v^2 dv \quad (20)$$

The escape fraction is defined by the ratio,

$$\alpha = \frac{\hat{R}_{esc}}{\hat{Q}} \quad (21)$$

where  $\hat{Q} = Q/N_O N_H$  and  $\hat{R}_{esc} = R_{esc}/N_O N_H$ . These collision rates, rate coefficients, and escape fractions are shown in Table 1 and Table 2 for H and D escape from Venus and in Table 3 and Table 4 for H and D escape from Mars. There is a slight increase in the total collision rates with increasing oxygen temperature. Since the cross section decreases with increasing energy, the average of the cross section (the  $y$  integral in (19)) decreases with increasing temperature, but the temperature dependent factor in front of the integral increases with temperature, and the net effect is that the collision

Table 1. Escape Fraction of H on Venus

| $T_O$ , K | $\hat{Q}^a$ | $\hat{R}_{esc}$ | $\alpha^b \times 10^2$ | $\alpha_{iso}^c \times 10^2$ |
|-----------|-------------|-----------------|------------------------|------------------------------|
| 5,000     | 29.34       | 0.0434          | 0.148                  | 0.897                        |
| 10,000    | 33.78       | 0.4134          | 1.22                   | 7.18                         |
| 15,000    | 37.33       | 1.043           | 2.79                   | 16.0                         |
| 20,000    | 40.36       | 1.762           | 4.37                   | 24.4                         |
| 29,113    | 45.01       | 3.081           | 6.85                   | 36.9                         |
| 35,000    | 47.61       | 3.891           | 8.17                   | 43.4                         |

<sup>a</sup> $\hat{Q}$  and  $\hat{R}_{esc}$  are in units of  $10^{-10}$   $\text{cm}^3 \text{s}^{-1}$ .

<sup>b</sup>Escape fraction  $\alpha = \hat{R}_{esc}/\hat{Q}$ .

<sup>c</sup>Escape fraction  $\alpha_{iso}$  is calculated with  $\sigma(E, \theta) = \sigma_{tot}(E)/4\pi$ .

rate increases with temperature. The escape rate coefficients and the escape fractions increase dramatically with increasing oxygen temperature, characteristic of a process with activation energy, which is a good analogy for the escape process. The last columns in the tables show the results with the isotropic approximation for the differential cross section. It is clear that estimates of nonthermal distributions in planetary exospheres and escape fractions require an accurate account of the dynamics of collision processes.

## 5. H and D Escape Fluxes From Venus

The escape rate coefficients are employed in the estimates of H and D escape fluxes from Venus. The calculation of the escape flux follows the formalism by Shizgal and Lindensfeld [1982]. The flux is given by the altitude integration of the form

$$F = \int_0^\infty w(z) \hat{R}_{esc} N_O(z) N_H(z) dz \quad (22)$$

where  $w(z)$  is the escape probability given by

$$w(z) = \frac{1}{2} E_2[z(y)] \quad (23)$$

$$y = \sigma_{O-H} \int_0^z N_O(z) dz \quad (24)$$

Table 2. Escape Fraction of D on Venus

| $T_O$ , K | $\hat{Q}^a$ | $\hat{R}_{esc}$ | $\alpha^b \times 10^2$ | $\alpha_{iso}^c \times 10^2$ |
|-----------|-------------|-----------------|------------------------|------------------------------|
| 5,000     | 26.45       | 0.00900         | 0.0340                 | 0.262                        |
| 10,000    | 31.69       | 0.1827          | 0.580                  | 4.27                         |
| 15,000    | 35.75       | 0.5766          | 1.61                   | 11.6                         |
| 20,000    | 39.14       | 1.084           | 2.77                   | 19.3                         |
| 29,113    | 44.19       | 2.087           | 4.27                   | 31.5                         |
| 35,000    | 46.65       | 2.684           | 5.75                   | 37.8                         |

<sup>a</sup> $\hat{Q}$  and  $\hat{R}_{esc}$  are in units of  $10^{-10}$   $\text{cm}^3 \text{s}^{-1}$ .

<sup>b</sup>Escape fraction  $\alpha = \hat{R}_{esc}/\hat{Q}$ .

<sup>c</sup>Escape fraction  $\alpha_{iso}$  is calculated with  $\sigma(E, \theta) = \sigma_{tot}(E)/4\pi$ .

**Table 3.** Escape Fraction of H on Mars

| $T_O$ , K | $\hat{Q}^a$ | $\hat{R}_{esc}$ | $\alpha^b \times 10^2$ | $\alpha_{iso}^c \times 10^2$ |
|-----------|-------------|-----------------|------------------------|------------------------------|
| 500       | 23.77       | 0.9893          | 4.16                   | 5.12                         |
| 1,000     | 24.52       | 1.222           | 4.98                   | 8.86                         |
| 2,000     | 25.90       | 1.780           | 6.87                   | 17.3                         |
| 5,000     | 29.34       | 3.491           | 11.9                   | 38.3                         |
| 10,000    | 33.78       | 5.739           | 17.0                   | 57.6                         |
| 15,000    | 37.33       | 7.451           | 20.0                   | 67.7                         |
| 20,000    | 40.36       | 8.847           | 21.9                   | 73.9                         |
| 29,113    | 45.01       | 10.92           | 24.3                   | 80.6                         |
| 35,000    | 47.61       | 12.05           | 25.3                   | 83.3                         |

<sup>a</sup> $\hat{Q}$  and  $\hat{R}_{esc}$  are in units of  $10^{-10} \text{ cm}^3 \text{ s}^{-1}$

<sup>b</sup>Escape fraction  $\alpha = \hat{R}_{esc}/\hat{Q}$

<sup>c</sup>Escape fraction  $\alpha_{iso}$  is calculated with  $\sigma(E, \theta) = \sigma_{tot}(E)/4\pi$ .

is the "optical depth" of the overlying atmosphere. In (23),  $E[z(y)]$  is the exponential integral. The cross section in the definition of  $y$  in (24) is a hard sphere cross section equal to  $60 \text{ \AA}^2$ . The escape probability tends to 0 rapidly for altitudes below the exobase and tends to 1/2 at high altitudes. For the particular applications here,  $w(z)$  is essentially the asymptotic value of 1/2, so that the value of  $\sigma_{O-H}$  is essentially irrelevant. In this way, the present model includes implicitly collisions of nonthermal  $H^*$  and  $D^*$  with the thermal atomic oxygen background, and not every hot atom produced escapes.

Density and temperature profiles for thermal (or cold) H, D, and O are required as well as the density and temperature profiles for hot  $O^*$  for day and night conditions. These profiles determine the altitude variation of the escape fluxes. A pair of thermal H densities for day and night conditions were derived from *Brinton et al.* [1980] in the manner of *Kumar et al.* [1980]. The nighttime and daytime temperatures were taken as 110 and 300 K which give scale heights of 102 and 279 km, respectively. The densities at 165 km were taken from Figure 3 of *Brinton et al.* [1980], giving the profiles  $N_H(z) = 4.5 \times 10^4 \exp(-z/279)$  and  $N_H(z) = 5 \times 10^6 \exp(-z/102)$  for day and night, respectively. The densities are in  $\text{cm}^{-3}$  and the altitude  $z$  is in km. The night profile fits very well the straight line of Figure 2 of *Brinton et al.* [1980]. The profile in Figure 3 of that paper does not correspond to 285 K as claimed. The day profile chosen here agrees with the cold hydrogen profile in Figure 3 of *Nagy et al.* [1981]. A second pair of H profiles were taken from Figure 7 of the more recent work of *Hartle et al.* [1996]. From the high-altitude portions of these profiles for night conditions, temperatures of 454 and 164 K were estimated for solar minimum and solar maximum, respectively.

The deuterium densities were determined by using one half the scale heights employed for the hydrogen densities. The density profile was fixed by setting the density at 150 km to be 0.025 times the hydrogen densities at that altitude [*Hartle et al.*, 1996]. For the

densities derived from *Brinton et al.* [1980], we get  $N_D(z) = 1.19 \times 10^3 \exp[-(z-150)/139.5]$  for day and  $N_D(z) = 1.48 \times 10^3 \exp[-(z-150)/51.2]$ . For the nighttime hydrogen densities of *Hartle et al.* [1996], we get  $N_D(z) = 1.84 \times 10^3 \exp[-(z-150)/201.5]$  for solar minimum and  $N_D(z) = 5.05 \times 10^4 \exp[-(z-150)/75.5]$  for solar maximum.

The cold oxygen profiles for night and day conditions were taken from data at high altitudes in Tables 3a and 3b, respectively, of *Hedin et al.* [1983]. These are given analytically by  $8.94 \times 10^{12} \exp(-z/19.17)$  for day and  $1.98 \times 10^{10} \exp(-z/8.4459)$  for night. Two sets of hot  $O^*$  profiles were employed. The first set was taken from Figure 3 for day and Figure 4 for night in the paper by *Nagy et al.* [1981]. A second single profile for solar maximum conditions was taken from Figure 4 of *Nagy et al.* [1990]. This profile lies between the other two profiles.

It is expected that in the vicinity of the exobase, where there are many collisions, the oxygen temperature would be essentially the temperature of the thermal background. The escape rate coefficients would be very small, and there is very little contribution to the nonthermal escape fluxes from collisions near the exobase. At higher altitudes, where the collision rate is lower, the hot oxygen atoms are not completely thermalized and the oxygen temperature is expected to increase rapidly and tend toward the temperature equivalent to the exothermicity of the dissociative recombination reaction. In this paper, we have added together the barometric fits of the hot and cold O density profiles together to give a composite density; that is,

$$N_O(z) = N_c e^{-z/H_c} + N_h e^{-z/H_h} \quad (25)$$

where  $c$  refers to cold and  $h$  refers to hot. The temperature profile for oxygen is then assumed to be given qualitatively by the local scale height; that is,

$$T_O(z) = -\frac{m_O g}{k} \frac{1}{N_O} \frac{dN_O}{dz} \quad (26)$$

**Table 4.** Escape Fraction of D on Mars

| $T_O$ , K | $\hat{Q}^a$ | $\hat{R}_{esc}$ | $\alpha^b \times 10^2$ | $\alpha_{iso}^c \times 10^2$ |
|-----------|-------------|-----------------|------------------------|------------------------------|
| 1,000     | 20.35       | 0.0484          | 0.238                  | 1.09                         |
| 2,000     | 22.17       | 0.2494          | 1.13                   | 6.06                         |
| 5,000     | 26.45       | 1.321           | 4.99                   | 26.6                         |
| 10,000    | 31.69       | 3.026           | 9.55                   | 48.8                         |
| 15,000    | 35.75       | 4.382           | 12.3                   | 60.6                         |
| 20,000    | 39.14       | 5.505           | 14.1                   | 67.6                         |
| 29,113    | 44.19       | 7.160           | 16.2                   | 75.1                         |
| 35,000    | 46.65       | 8.023           | 17.2                   | 78.3                         |

<sup>a</sup> $\hat{Q}$  and  $\hat{R}_{esc}$  are in units of  $10^{-10} \text{ cm}^3 \text{ s}^{-1}$ .

<sup>b</sup>Escape fraction  $\alpha = \hat{R}_{esc}/\hat{Q}$ .

<sup>c</sup>Escape fraction  $\alpha_{iso}$  is calculated with  $\sigma(E, \theta) = \sigma_{tot}(E)/4\pi$ .

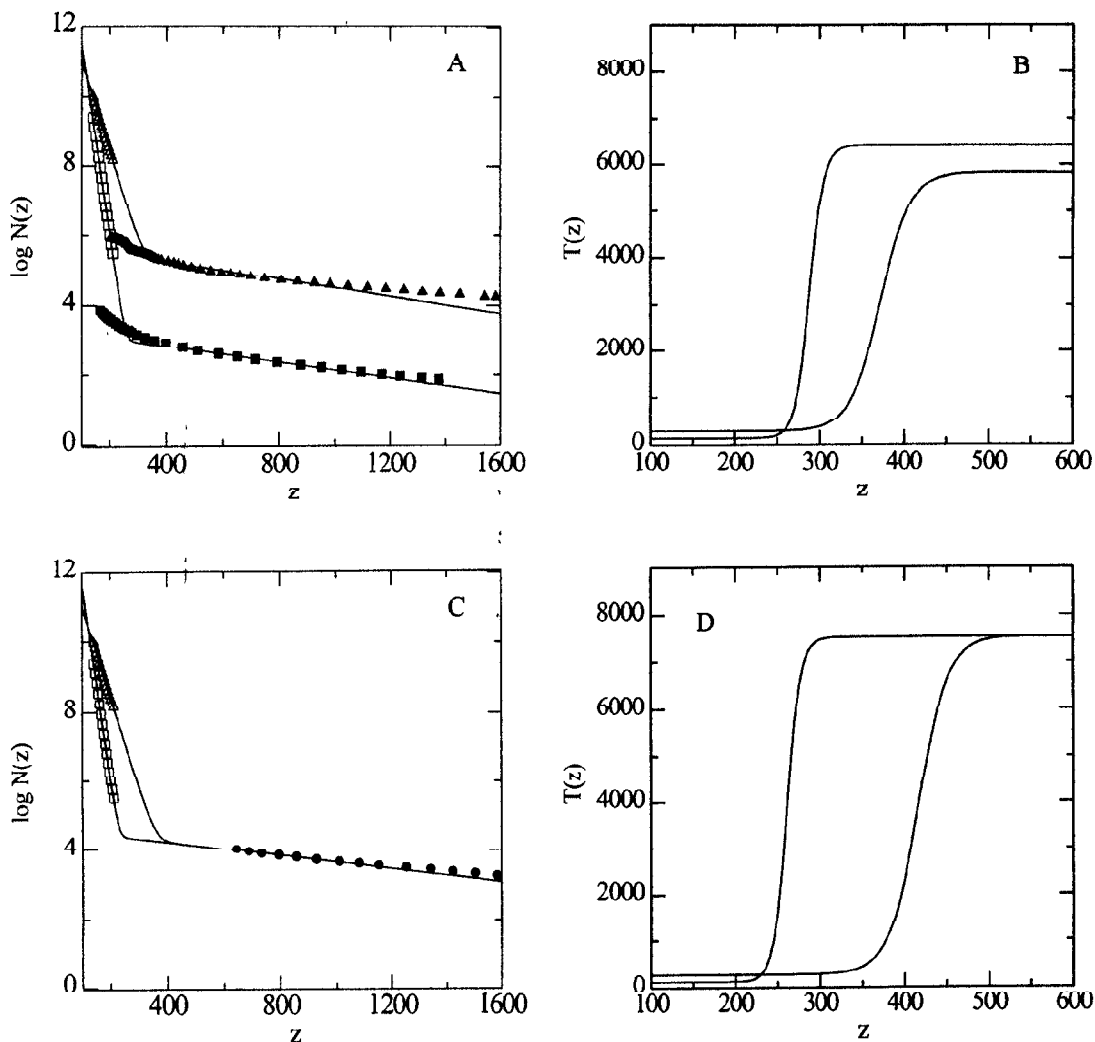


**Figure 5.** (a) Oxygen density profiles: Open triangles and open squares are the cold oxygen densities from *Hedin et al.* [1983] for day and night, respectively. Solid triangles and solid squares are the hot oxygen densities from *Nagy et al.* [1981] for day and night, respectively. The solid curves are the sum of the hot and cold densities, equation (25), drawn with the semilogarithmic fits to the profiles. (b) Temperature profiles (given by (26)) with the densities in Figure 5a for day (top curve) and night (bottom curve). (c) Same cold oxygen densities as in Figure 5a, but with the hot oxygen profile from *Nagy et al.* [1990] (solid circles). (d) Temperature profiles (given by (26)) with the densities in Figure 5c for day (top curve) and night (bottom curve).

as shown in Figure 5. The fitting procedure for the two sets of density profiles is shown in Figures 5a and 5c, and the corresponding temperature profiles are shown in Figures 5b and 5d. This is clearly an approximation, but it does implicitly include some collisionality, and the oxygen temperatures shown in the figures increase rapidly from thermal values to values close but considerably less than the exothermicity of the dissociative recombination reaction of 2.5 eV equivalent to  $\sim 29,000$  K. Nonthermal distributions obtained from a Boltzmann equation are required to justify these profiles. However, in the absence of such calculations, the

profiles defined by (25) and (26) appear quite reasonable. Only the lower-altitude portions of these profiles contribute to the escape fluxes. The integral in (22) converges rather quickly, at altitudes below about several hundred kilometers. The day profiles vary more rapidly than the night profiles, and both approach a similar limiting temperature at high altitudes. The altitude range for the thermalization of hot oxygen is very narrow.

An approximate solution of the Boltzmann equation, (1), with species 1 representing hot oxygen and species 2 thermal (or cold) oxygen, is described in the appendix.

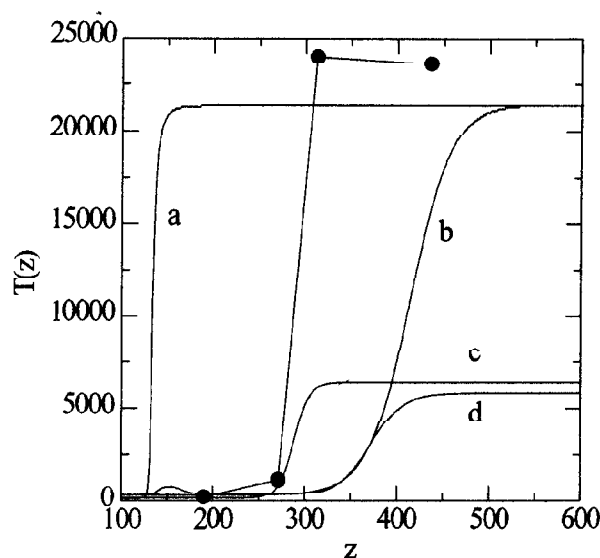


**Figure 6.** Temperature profiles for oxygen on Venus. The curve with the solid circles is derived from the distributions in Figure 6 of *Hodges* [1993b]. Curves a and b are determined with equation (A4) for day and night conditions, respectively. Curves c and d are profiles reproduced from Figure 5b.

Figure 6 shows a comparison of several different temperature profiles. Curves a and b are the results of the calculation in the appendix for day and night conditions, respectively. Curves c and d, given by (25) and (26), are reproduced from Figure 5b. The solid circles depict the temperature profile extracted from the  $O^*$  distributions reported by *Hodges* [1993b] for day conditions. Only results from the lowest altitudes could be extracted from his results, as the distributions at higher altitudes contain too much "noise" from the Monte Carlo simulations. The ion and neutral O densities in his work differ from those chosen here, and the exospheric situation treated there cannot be directly compared with the simple BGK [*Bhatnager et al.*, 1954] model used in the appendix. Nevertheless, the results in Figure 6 indicate the trend to be expected for the thermalization of hot oxygen in the vicinity of the exobase and above. The comparison shown in Figure 6 suggests that the use of (25) and (26) is justified. The hot oxygen distributions modeled here as Maxwellians with the temperature profiles in Figures 5b and 5d are cooler than the distributions reported by *Hodges* [1993b] with thermalization. If the oxygen distributions are indeed hotter, which they may be, the energization of H and D may be greater than reported in this paper.

Results for the H and D escape fluxes for the choice of density and temperature profiles discussed here are shown in Table 5 and Table 6. The fractionation factor in the tables is defined as

$$f = \frac{1}{\langle D/H \rangle} \frac{F_D}{F_H} \quad (27)$$

**Table 5.** Escape Fluxes From Venus

| O and H Densities | $F_H^{(iso)}$      | $F_H$              | $F_D$ | $f$   |
|-------------------|--------------------|--------------------|-------|-------|
| A1 and H-day      | $2.23 \times 10^5$ | $3.74 \times 10^4$ | 70.1  | 0.075 |
| A2 and H-night    | $1.07 \times 10^7$ | $1.79 \times 10^6$ | 3160  | 0.071 |
| B and H-day       | $1.22 \times 10^6$ | $2.02 \times 10^5$ | 332   | 0.066 |
| B and H-night     | $1.55 \times 10^5$ | $2.56 \times 10^4$ | 30.7  | 0.048 |

$F$  is flux and  $f$  is fractionation factor. The A1 oxygen profile is based on the cold oxygen day profile in Table 3a of *Hedin et al.* [1983] and the hot oxygen day profile is from Figure 3 of *Nagy et al.* [1981]. The A2 oxygen profile is based on the cold oxygen night profile in Table 3b of *Hedin et al.* [1983], and the hot oxygen night profile is from Figure 4 of *Nagy et al.* [1981]. The temperature profiles are derived from equations (25) and (26). The B profile is based on the hot oxygen profile from Figure 4 of *Nagy et al.* [1990]. The cold profiles are as for A1 and A2. The hydrogen day and night profiles are from *Brinton et al.* [1980]. The deuterium densities are derived from the hydrogen densities by halving the scale heights and adjusting the densities to be 0.025 times the corresponding hydrogen densities.

where  $\langle D/H \rangle = 0.025$  is the globally average abundance ratio [*Hartle et al.*, 1996]. For  $f = 1$  there is no fractionation and as  $f \rightarrow 0$ , the fractionation of D over H becomes more efficient. From Table 5, it is clear that the assumption of an anisotropic differential cross section overestimates the flux by a factor close to 6. The escape fluxes vary considerably, as there is a strong dependence on the profiles, which are only representative. The H and D escape fluxes reported here are comparable but somewhat lower than the values of  $3.5 \times 10^6$  and  $3.1 \times 10^4 \text{ cm}^{-2} \text{ s}^{-1}$ , respectively, reported by *Gurwall and Yung* [1993]. Their work is incomplete, as they used a cross section at only one energy. It is not clear how the escape fluxes were estimated, as an altitude average analogous to (22) was not discussed in their paper. The higher fluxes for the profiles in Ta-

**Table 6.** Escape Fluxes From Venus, Second Set of H Densities

| O Density | H Density | $F_H$              | $F_D$              | $f$   |
|-----------|-----------|--------------------|--------------------|-------|
| A1        | Smin      | $3.06 \times 10^7$ | $1.13 \times 10^5$ | 0.148 |
| A1        | Smax      | $1.40 \times 10^6$ | $3.60 \times 10^3$ | 0.103 |
| A2        | Smin      | $6.41 \times 10^5$ | $1.86 \times 10^3$ | 0.116 |
| A2        | Smax      | $2.25 \times 10^4$ | $1.49 \times 10^2$ | 0.265 |

The A1 and A2 oxygen profiles are derived as described in Table 5. The hydrogen densities denoted by Smin and Smax correspond to the profiles in Figure 7 of *Hartle et al.* [1996] for solar minimum and solar maximum conditions on the nightside. The deuterium densities are derived from the hydrogen densities by halving the scale heights and adjusting the density at 150 km to 0.025 times the corresponding hydrogen densities

ble 6 relative to those in Table 5 arise from the higher densities used in estimating the fluxes in Table 6. The corresponding fractionation factors are larger in Table 6 than in Table 5. The fractionation ratios are smaller than the value  $f = 0.47$  suggested by *Gurwell and Yung* [1993], who used  $\langle D/H \rangle = 0.014$ .

The actual hot atom distributions  $H^*$ ,  $D^*$  as well as  $O^*$  should be determined from a solution of the appropriate Boltzmann equations to justify steady nonthermal distributions. This is a formidable problem, and such an undertaking is not justified at present, given the lack of detailed data, which might be forthcoming from the upcoming Mars missions. *Rodriguez et al.* [1984] used hot atom sources in a solution of the collisionless Boltzmann equation, so that nonlocal diffusion in the planetary gravitational field was taken into account in the determination of steady, nonthermal distributions. Collisional thermalization was not included for  $H^*$  or  $D^*$ , but some type of hot atom transport modeled after radiative transfer models was included for  $O^*$ . *Kumar et al.* [1980] discussed thermalization of hot H and D in collision with  $CO_2$  and O in very qualitative terms, in terms of average collision numbers. The density of  $CO_2$  appears to be too low to contribute much to the thermalization. *Gurwell and Yung* [1993] mention that their model does not include multiple scattering of  $O^*$  with H and D; that is, collisional thermalization was not included in their work. However, these authors recognize that the collisional energy transfer process that can be considered to thermalize hot atoms is also responsible for producing them. The present model imposes steady  $H^*$  and  $D^*$ , distributions and the Boltzmann equation (1) cannot be used in the present form to determine the actual distribution, as the collision operator is responsible for both the energization and deexcitation of these hot atoms as noted by *Gurwell and Yung* [1993].

The present approach is local, so that the effects of transport in the gravitational field are not included. The collisional production of fast atoms is based on the Boltzmann equation, (1), which is rewritten in the form

$$\frac{\partial f_H}{\partial t} = f_H^{(M)} Z_{(+)}(v) - f_H Z_{(-)}(v) \quad (28)$$

The long-time solution of this equation with some background  $O^*$  Maxwellian distribution would give a steady hydrogen Maxwellian distribution at the oxygen temperature. This would lead to larger escape fluxes than reported here. The present approach has assumed that the loss collision frequency,  $Z_{(-)}(v)$ , in (28) can be replaced by the average value  $Q$  given by (9). The distribution equation (10) is then obtained by assuming some steady state,  $\partial f_H / \partial t = 0$ . An alternate choice would be to retain the velocity dependence in  $Z_{(-)}(v)$  and get, for the steady hot atom distribution,

$$f_H = \frac{F_H^{(M)} Z_{(+)}(v)}{Z_{(-)}(v)} \quad (29)$$

Either choice is not rigorously justified, as the steady state at infinite time (with the present local model) would be complete equilibration of H and O. However, for comparison, (29) was used to estimate the escape fractions for the escape of H from Venus, with  $P(v)$  appropriately renormalized. For night conditions and the three altitudes, 270, 280, and 300 km corresponding to oxygen temperatures of 5750, 6917, and 7465 K, respectively, the escape fractions  $\alpha$  are reduced by approximately 40% from the results with  $\hat{Q}$  in place of  $Z_{(-)}(v)$ . *Hodges* [1993b] and *Hodges and Breig* [1991, 1993] calculate escape rate coefficients with the difference of the collision frequencies, i.e., the full collision operator, (2). Their approach cannot be interpreted as based on a product distribution, as for this case, there are both positive and negative contributions to the escape fractions; the product velocity distribution implicit in their work would have negative parts. It is not clear what the relationship is between these different approaches, and a more detailed consideration of the kinetic theory is warranted.

## 6. Discussion of Results

The present results have demonstrated the importance of the proper collision dynamics in the calculation of nonthermal escape fluxes. Accurate O-H and O-D differential cross sections [*Shizgal*, 1999] were employed in the calculation of the distribution of energetic H and D. The escape fluxes of H and D were calculated for several representative density profiles and found to be significant, as high as  $3 \times 10^7 \text{ cm}^{-2} \text{ s}^{-1}$  for H and  $10^5 \text{ cm}^{-2} \text{ s}^{-1}$  for D. These results were obtained for particular densities and do not represent a global average. Nevertheless, the results suggest that energization of H and D by hot oxygen impact is an important escape mechanism. Also, the fractionation ratios varied from 0.048 to 0.265, lower than the value of 0.47 suggested by *Gurwell and Yung* [1993]. The fractionation ratio by *Gurwell and Yung* [1993] is not based on actual escape fluxes but inferred from their estimates of escape fractions. The work of *Cooper et al.* [1984] did not consider O-D collisions, and fractionation ratios were not reported.

*Hodges* [1993b] calculated, with the full collision operator (equation (2)), the escape rate ratios  $\gamma_D/\gamma_H$  for charge exchange, and showed that these were significantly below the corresponding ratios reported by *Gurwell and Yung* [1993] for energetic oxygen impact [*Hodges*, 1993b, Figure 4]. He concluded that charge exchange encourages high isotopic fractionation, but energetic oxygen impact does not. It is important to note that the ratio  $\gamma_D/\gamma_H$  is a ratio of rate coefficients or escape fractions and is not the fractionation ratio as defined by (27), which is expressed in terms of escape fluxes. A similar comparison using the escape fractions in Tables 1 and 2 gives ratios,  $\alpha_D/\alpha_H$ , that vary from 0.23 to 0.70. The actual fractionation ratios for ener-

getic oxygen impact defined by (27) reported in Tables 5 and 6 are in the range 0.048 - 0.265, comparable to the results for charge exchange and much smaller than the escape fraction ratios. The early work by *McElroy et al* [1982] suggested that the isotopic fractionation was 0.

*Hodges* [1993b] also determined the energetic oxygen distribution from a Monte Carlo simulation of the exosphere. He demonstrated that the effect of O\*-O collisions thermalizes the hot energy tail of the oxygen distribution function, and hence he concluded that this mitigates against H and D escape by energetic oxygen impact. An examination of the distributions in his Figures 6 and 7 verifies that the low-velocity portions of the distributions for the four lowest altitudes are Maxwellian at approximately 250 K, consistent with the scale height of the thermal oxygen density distribution in Figure 5. The integral of this Maxwellian gives the density of thermal oxygen, which when subtracted from the integration of the full distribution of Figure 6 (with O-O collisions), gives the hot oxygen densities of  $1.4 \times 10^8$ ,  $2 \times 10^6$ , and  $1.4 \times 10^6$  cm<sup>-3</sup> for 190, 270, and 310 km, respectively. The corresponding densities at the same altitudes without O-O collisions (Figure 7) are  $6.7 \times 10^8$ ,  $2 \times 10^7$ , and  $5.4 \times 10^6$  cm<sup>-3</sup>, respectively. Therefore the collisional thermalization has reduced the hot oxygen densities by factors of 4-10. However, the hot oxygen densities obtained in this way are much larger than those employed here, which are of the order of  $10^4$  -  $10^5$  cm<sup>-3</sup>. Moreover, the oxygen temperatures used in the present calculations are lower than the temperature profile extracted from the distributions in Figure 6 of *Hodges* [1993b] and shown in Figure 6 of this paper. Consequently, the oxygen distributions, with O\*-O collisions reported by *Hodges* [1993b], would yield H and D escape fluxes larger than those reported in Tables 5 and 6. Energetic oxygen impact remains an important process to consider in addition to charge exchange and the flux due to the charge separation electric field [*Hartle et al.*, 1996]. Further work toward the actual nonequilibrium H\* and D\* distributions, obtained from Boltzmann equation models and estimates of globally averaged escape fluxes, is ongoing.

### Appendix: Hot Oxygen Temperature Profile, Venus

*Hodges* [1993b] carried out a Monte Carlo simulation to determine the distributions including the effects of subsequent thermalization owing to collisions with thermal oxygen. We employ a much simpler model here than that employed by *Hodges* [1993b] and consider a solution of the Boltzmann equation with the approximation of the collision operator introduced by *Bhatnager et al.* [1954] and referred to as the BGK approximation. The collision operator describes collisions between hot and thermal oxygen atoms, considered as two distinct species. The hot O\* source distribution,  $S(v)$ , is the one shown in Figure 3 of *Gurwell and Yung* [1993]. We

use a Chapman-Enskog type solution of the Boltzmann equation [*Shizgal and Karplus*, 1970; *Shizgal and Lindenfeld*, 1979; *Napier and Shizgal*, 1995; *Shizgal and Napier*, 1996] and assume that the time dependence of the distribution function is implicit through the density; that is,  $\partial f / \partial t = (df/dN_h)(dN_h/dt)$ , where  $N_h(z)$  is the density of "hot" oxygen,  $dN_h/dt = K_r N_i^2$ ,  $K_r = 10^{-7}$  cm<sup>3</sup> s<sup>-1</sup> is the dissociative recombination rate coefficient [*Guberman*, 1988], and  $N_i(z)$  is the O<sub>2</sub><sup>+</sup> density. The collision operator is written as

$$J[f] = N_h(z) \hat{J}[F] = -N_h(z) \frac{F - F^{(M)}}{\tau(z)} \quad (\text{A1})$$

where  $f = N_h(z)F$  and the second equality is the BGK approximation of the collision operator. The quantity  $\tau(z)$  is a relaxation time and is chosen as the reciprocal of the elastic collision frequency (see (7)); that is,

$$\tau(z) = \frac{1}{N_c(z) \pi d^2} \sqrt{\frac{\pi \mu}{8k_B T_{eff}(z)}} \quad (\text{A2})$$

where  $N_c(z)$  is the density of "cold" or thermal oxygen. The BGK approximation effectively replaces the spectrum of relaxation times of the collision operator with one representative value. If these assumptions are introduced into (1), a steady state distribution function is obtained in the form

$$F(z, v) = \frac{N_h(z)}{N_*(z)} F^{(M)}(v) + \frac{\tau(z) K_r N_i^2(z)}{N_*(z)} S(v) \quad (\text{A3})$$

where  $N_*(z) = \tau(z) K_r N_i^2(z) + N_h(z)$ . The temperature of the energetic oxygen atoms, which now includes thermalization with the background thermal oxygen, is defined by  $T(z) = \frac{1}{3k_B} \int F(z, v) m v^2 dv$  and is given by

$$T(z) = \frac{N_h(z)}{N_*(z)} T_c + \frac{\tau(z) K_r N_i^2(z)}{N_*(z)} T_h \quad (\text{A4})$$

We choose a hard sphere cross section ( $\pi d^2$ ) for O-O\* collisions of  $20 \text{ \AA}^2$  [*Hodges*, 1993b], which yields  $\tau(z) K_r = 897 \text{ s}^{-1}/N_c(z)$  with  $N_c$  in cm<sup>-3</sup>. To complete this simple calculation, we require the three density profiles,  $N_c(z)$ ,  $N_h(z)$ , and  $N_i(z)$ . Notice that this formalism is local, and the density  $N_h(z)$  is a parameter. The cold oxygen densities for day and night conditions are taken from *Brinton et al.* [1980] and are given by the approximate analytic fits,  $\log N_c^{(\text{day})}(z) = 13.118 - 0.02670z$  and  $\log N_c^{(\text{night})}(z) = 18.9235 - 0.06858z$ , with  $N_c(z)$  in units of cm<sup>-3</sup> and  $z$  in km. The temperature  $T_h$  is determined from the average of  $m v^2/2$  with  $S(v)$  and is 21,450 K. The temperature  $T_c$  is taken from the scale height corresponding to  $N_c$  and is 284 K for day and 132 K for night. The hot oxygen densities are taken from *Nagy et al.* [1981] and are given by the approximate analytic fits,  $\log N_h^{(\text{day})}(z) = 5.762 - 0.001273z$  and  $\log N_h^{(\text{night})}(z) = 3.283 - 0.001599z$  with  $N_h(z)$  in units of cm<sup>-3</sup> and  $z$  in km. The ion density profile is taken from *Nagy et al.* [1980].

**Acknowledgments.** This research is supported in part by a grant from the Natural Sciences and Engineering Research Council of Canada. I am pleased to acknowledge the assistance of K. Marubashi and T. Tanaka for arranging my visit to the Communications Research Laboratory where a substantial portion of this work was done.

Michel Blanc thanks both referees for their assistance in evaluating this paper.

## References

- Armstrong, P. S., S. J. Lipson, J. A. Dodd, J. R. Lowell, W. A. M. Blumberg and R. M. Nadile, Highly rotationally excited NO(v,J) in the thermosphere from CIRRIS 1A limb radiance measurements, *Geophys. Res. Lett.*, **21**, 2425-2428, 1994.
- Bhatnager, P. L., E. P. Gross, and M. Krook, A model for collision processes in gases, I, Small amplitude processes in charged and neutral one component systems, *Phys. Rev.*, **94**, 511-525, 1954.
- Brinton, H. C., H. A., Taylor, H. B. Niemann, H. G. Mayr, A. F. Nagy, T. E. Cravens, and D. F. Strobel, Venus nighttime hydrogen bulge, *Geophys. Res. Lett.*, **7**, 865-868, 1980.
- Chamberlain, J. W., Charge exchange in planetary corona: Its effect on the distribution and escape of hydrogen, *J. Geophys. Res.*, **82**, 1-9, 1977.
- Chapman, S., and T. G. Cowling, *The Mathematical Theory of Nonuniform Gases*, Cambridge Univ. Press, New York, 1970.
- Cooper, D. L., J. H. Yee, and A. Dalgarno, Energy transfer in oxygen hydrogen collisions, *Planet. Space Sci.*, **32**, 825-830, 1984.
- Donahue, T. M., D. H. Grinspoon, R. E. Hartle, and R. R. Hodges Jr., *Ion/neutral escape of hydrogen and deuterium: Evolution of water*, in *Venus II Geology, Geophysics, Atmosphere and Solar Wind Environment*, edited by S. W. Bougher, D. M. Hunten, and R. J. Phillips, pp. 385-414, Univ. of Ariz Press, Tucson, 1997.
- Fahr, H. J., and B. Shizgal, Modern exospheric theories and their observational relevance, *Rev. Geophys.*, **21**, 75-124, 1983.
- Fox, J. L., The production and escape of N atoms on Mars, *J. Geophys. Res.*, **98**, 3297-3310, 1993.
- Fox, J. L., and A. Hać, The  $N^{15}/N^{14}$  isotope fractionation in the dissociative recombination of  $N_2^+$ , *J. Geophys. Res.*, **102**, 9191-9204, 1997a.
- Fox, J. L., and A. Hać, Spectrum of hot O at the exobases of the terrestrial planets, *J. Geophys. Res.*, **102**, 24,005-24,011, 1997b.
- Gérard, J.-C., D. V. Bisikalo, V. I. Shematovich, and J. W. Duff, An updated model of hot nitrogen atom kinetics and thermospheric nitric oxide, *J. Geophys. Res.*, **102**, 285-294, 1997.
- Gombosi, T. A., *Gas Kinetic Theory*, Cambridge Univ. Press, New York, 1994.
- Guberman, S. L., The production of O( $^1$ D) from dissociative recombination of  $O_2^+$ , *Planet. Space Sci.*, **36**, 47-53, 1988.
- Gurwell, M. A., and Y. L. Yung, Fractionation of hydrogen and deuterium on Venus due to collisional ejection, *Planet. Space Sci.*, **41**, 91-104, 1993.
- Hartle, R. E., T. M. Donahue, J. M. Grebosky, and H. G. Mayr, Hydrogen and deuterium in the thermosphere of Venus: Solar cycle variations and escape, *J. Geophys. Res.*, **101**, 4525-4538, 1996.
- Hays, P. B., and J. C. G. Walker, Doppler profiles of the 5577 Å<sup>2</sup> airglow, *Planet. Space Sci.*, **14**, 1331-1337, 1971.
- Hedin, A. E., H. B. Niemann, W. T. Kasprzak, and A. Seiff, Global empirical model of the venus thermosphere, *J. Geophys. Res.*, **88**, 73-83, 1983.
- Hodges, R. R., Jr., Collision cross sections and diffusion parameters for H and D in atomic oxygen, *J. Geophys. Res.*, **98**, 3799-3805, 1993a.
- Hodges, R. R., Jr., Isotopic fractionation of hydrogen in planetary exospheres due to ionosphere-exosphere coupling: Implications for Venus, *J. Geophys. Res.*, **98**, 10,833-10,838, 1993b.
- Hodges, R. R., Jr., and E. L. Breig, Ionosphere - exosphere coupling through charge exchange and momentum transfer in hydrogen-proton collisions, *J. Geophys. Res.*, **96**, 7697-7708, 1991.
- Hodges, R. R., Jr., and E. L. Breig, Charge transfer and momentum exchange in exospheric D-H<sup>+</sup> and H-<sup>+</sup>D collisions, *J. Geophys. Res.*, **98**, 1581-1588, 1993.
- Hunten, D. M., Kuiper prize lecture: Escape of atmospheres, ancient and modern, *Icarus*, **85**, 1-20, 1991.
- Ip, W.-H., On a hot oxygen corona on Mars, *Icarus*, **76**, 135-145, 1988.
- Kharchenko, V., J. Tharmel, and A. Dalgarno, Kinetics of thermalization of fast nitrogen atoms beyond the hard sphere approximation, *J. Atmos. Sol. Terr. Phys.*, **59**, 107-115, 1997.
- Knudsen, W. C., Escape of <sup>4</sup>He and fast O atoms from Mars and inferences on the <sup>4</sup>He mixing ratio, *J. Geophys. Res.*, **78**, 8049-8054, 1973.
- Kumar, S., D. M. Hunten, and J. B. Pollack, Nonthermal escape of hydrogen and deuterium from Venus and implications for the loss of water, *Icarus*, **55**, 369-389, 1980.
- Lammer, H., and S. J. Bauer, Nonthermal atmospheric escape from Mars and Titan, *J. Geophys. Res.*, **96**, 1819-1825, 1991.
- Lie-Svendensen, O., M. H. Rees, and E. C. Whipple, The kinetics of hot nitrogen atoms in upper atmospheric neutral chemistry, *Planet. Space Sci.*, **39**, 929-943, 1991.
- Logan, J. A., and M. B. McElroy, Distribution functions for energetic oxygen atoms in the Earth's lower atmosphere, *Planet. Space Sci.*, **25**, 117-122, 1977.
- McElroy, M. B., M. J. Prather, and J. M. Rodriguez, Escape of hydrogen from Venus, *Science*, **215**, 1614-1615, 1982.
- Nagy, A. F., T. E. Cravens, S. G. Smith, H. A. Taylor Jr., and H. C. Brinton, Model calculations of the dayside ionosphere of Venus: Ionic composition, *J. Geophys. Res.*, **85**, 7795-7801, 1980.
- Nagy, A. F., T. E. Cravens, J. H. Yee, and A. I. F. Stewart, Hot oxygen atoms in the upper atmosphere of Venus, *Geophys. Res. Lett.*, **8**, 629-632, 1981.
- Nagy, A. F., J. Kim, and T. E. Cravens, Hot hydrogen and oxygen atoms in the upper atmospheres of Venus and Mars, *Ann. Geophys.*, **8**, 251-256, 1990.
- Napier, D. G., and B. D. Shizgal, Nonequilibrium effects in model reactive systems. The role of species temperatures, *Phys. Rev. E*, **52**, 3797-3811, 1995.
- Rodriguez, J. M., M. J. Prather, and M. B. McElroy, Hydrogen on Venus: Exospheric distribution and escape, *Planet. Space Sci.*, **32**, 1235-1255, 1984.
- Shizgal, B., Analysis of the dynamics of (H<sup>+</sup>,H) charge exchange collisions in the production of nonthermal H (abstract), *Eos Trans. AGU*, **66**, 1002, 1985.
- Shizgal, B., Hot hydrogen and deuterium in the exosphere of Venus, *Adv. Space Sci.*, **7**(12), 73-77, 1987.
- Shizgal, B. D., An analysis of O-H interaction potentials, O-H and O-D collision cross sections, and O-H vibrational states, *Planet. Space Sci.*, **47**, 163-174, 1999.
- Shizgal, B. D., and G. G. Arkos, Nonthermal escape of the atmospheres of Venus, Earth and Mars, *Rev. Geophys.*, **34**, 483-505, 1996.
- Shizgal, B., and J. M. Fitzpatrick, Temperature relaxation in a binary gas, I, Steady state solution, *J. Chem Phys.*, **63**, 131-137, 1975.

- Shizgal, B., and M. Karplus, Nonequilibrium contributions to the rate of reaction. Perturbation of the velocity distribution function, *J. Chem. Phys.*, *52*, 4262-4278, 1970.
- Shizgal, B., and M. Lindenfeld, The distribution function for hot  $O(^3P)$  atoms in the Earth's lower atmosphere, *Planet. Space Sci.*, *27*, 1321-1332, 1979.
- Shizgal, B., and J. M. Lindenfeld, A simple kinetic theory calculation of terrestrial atomic hydrogen escape fluxes induced by charge exchange collisions, *J. Geophys. Res.*, *87*, 853-858, 1982.
- Shizgal, B. D., and D. G. Napier, Nonequilibrium effects in reactive systems. The effect of reaction products and the validity of the Chapman-Enskog method, *Physica A*, *223*, 50-86, 1996.
- Viehland, L. A., Velocity distribution functions and transport coefficients of atomic ions in atomic gases by a Gram-Charlier approach, *Chem Phys.*, *179*, 71-92, 1994.
- Wallis, M. K., Exospheric density and escape fluxes of atomic isotopes on Venus and Mars, *Planet Space Sci.*, *26*, 949-953, 1978.
- Whipple, E. C., Use of the scattering kernel approach to certain gas kinetic problems, *Phys. Fluids*, *15*, 988-994, 1972.
- Whipple, E. C., Theory of reaction product velocity distribution, *J. Chem. Phys.*, *60*, 1346-1353, 1974.
- Whipple, E. C., T. E. Van Zandt, and C. H. Love, The kinetic theory of warm atoms; non-Maxwellian velocity distributions and resulting Doppler-broaden emission profiles, *J. Chem. Phys.*, *62*, 3204-3030, 1975.
- Yee, J. H., and A. Dalgarno, Energy transfer of  $O(^1S)$  atoms in collision with  $O(^3P)$  atoms, *Planet Space Sci.*, *33*, 825-830, 1985.

B. D. Shizgal, Department of Chemistry, University of British Columbia, 2036 Main Hall, Vancouver, B.C., Canada V6T 1Z4. (shizgal@theory.chem.ubc.ca)

(Received June 18, 1998, revised February 22, 1999; accepted March 18, 1999.)